made for the uncertainty due to the poorly known $CO_2$ pressure-induced coefficient.
26. D. D. Diner, *J. Atmos. Sci.* **35**, 2536 (1979).
27. We thank the Galileo Project management and engineering staff for their continuing support of NIMS. We especially acknowledge the efforts of the late C. Yeates, Galileo Science and Mission Design Manager. We have lost a resourceful scientist and a good friend in his untimely death. We are grateful to N. Ausman, Galileo Mission Director, and the Orbiter Engineering Team for providing crucial real-time commands to the spacecraft during the Venus flyby. The Science Requirements and Operation Planning staff (J. Dunne, K. Buxbaum, and V. Henderson) formulated the highly successful Venus flyby sequences, providing us the opportunity to collect the data reported here. The preparation and processing of these data required the expertise of many people including J. Anderson, T. Arakelian, K. Becker, V. Carrere, R. Chang-Diaz, K. Edwards, E. Eliason, J. Gardner, M. Hernandez, S. Lavoie, F. Leader, R. Lopez-Gautier, C. Mahoney, R. Mehlman, M. Segura, J. Torson, L. Wainio, and J. Yoshimizu. We are grateful to B. Bezard, D. Crisp, D. Hunten, A. Lacis, and W. Rossow for valuable discussion and comments. This work was supported under NASA contract NAS 7-100 with the Jet Propulsion Laboratory, California Institute of Technology.

23 May 1991; accepted 19 August 1991

# Galileo Ultraviolet Spectrometer Experiment: Initial Venus and Interplanetary Cruise Results

C. W. HORD, C. A. BARTH, L. W. ESPOSITO, W. E. MCCLINTOCK, W. R. PRYOR, K. E. SIMMONS, A. I. F. STEWART, G. E. THOMAS, J. M. AJELLO, A. L. LANE, R. W. WEST, B. R. SANDEL, A. L. BROADFOOT, D. M. HUNTEN, D. E. SHEMANSKY

**The Galileo Extreme Ultraviolet Spectrometer obtained a spectrum of Venus atmospheric emissions in the 55.0- to 125.0-nanometer (nm) wavelength region. Emissions of helium (58.4 nm), ionized atomic oxygen (83.4 nm), and atomic hydrogen (121.6 nm), as well as a blended spectral feature of atomic hydrogen (Lyman-β) and atomic oxygen (102.5 nm), were observed at 3.5-nm resolution. During the Galileo spacecraft cruise from Venus to Earth, Lyman-α emission from solar system atomic hydrogen (121.6 nm) was measured. The dominant source of the Lyman-α emission is atomic hydrogen from the interstellar medium. A model of Galileo observations at solar maximum indicates a decrease in the solar Lyman-α flux near the solar poles. A strong day-to-day variation also occurs with the 27-day periodicity of the rotation of the sun.**

ON 8 FEBRUARY 1990 THE EXTREME Ultraviolet Spectrometer (EUV) on the Galileo spacecraft obtained a spectrum of Venus in the wavelength range of 55 to 125 nm. After this encounter, the interplanetary cruise period from Venus in February 1990 to Earth in December 1990 was used for observations of atomic hydrogen Lyman-α (121.6-nm) radiation from the interplanetary medium. The EUV (*1*) has a mechanical collimator and a single-reflection Wadsworth optical system that uses a concave grating to feed a 128-pixel, bare microchannel plate detector. The resulting spectra have 3.5-nm spectral resolution for objects that fill the 0.87° by 0.17° field of view of the instrument. The spacecraft spin axis maintains an orientation that is within a few degrees of the sun while it is inside 1 astronomical unit (AU).

C. W. Hord, C. A. Barth, L. W. Esposito, W. E. McClintock, W. R. Pryor, K. E. Simmons, A. I. F. Stewart, G. E. Thomas, Laboratory for Atmospheric and Space Physics, University of Colorado, Boulder, CO 80309.
J. M. Ajello, A. L. Lane, R. W. West, Jet Propulsion Laboratory, California Institute of Technology, Pasadena, CA 91109.
B. R. Sandel, A. L. Broadfoot, D. M. Hunten, D. E. Shemansky, Lunar and Planetary Laboratory, University of Arizona, Tucson, AZ 85721.

The EUV is mounted on the spinning section of the spacecraft, and its field of view sweeps out a great circle 0.87° wide on the celestial sphere at about 3 rpm, passing through the north and south ecliptic poles in a plane perpendicular to the spacecraft spin axis. Commands to the EUV determine the fraction of the great circle observed and the number of bins (called sectors) into which that fraction is divided. During the Venus encounter individual photon events, together with a wavelength and a sky sector location, were stored on the spacecraft tape recorder for later playback to Earth. During the interplanetary cruise the photon events were integrated in the onboard memory of the EUV in a matrix of sector and wavelength knowledge, which was periodically read out.

During the Venus encounter EUV data were recorded for 75 min, 25 min of which contain the planet. The observed great circle was divided into 120 1.6° sectors: Venus filled 17 sky sectors as the spacecraft flew past at 22,000 to 29,000 km from the planet center. The disk-integrated dayglow spectrum of Venus (Fig. 1) shows several well-resolved emission lines. The feature at 121.6 nm (H Lyman-α) is due to resonance scattering of sunlight by atomic hydrogen. The feature near 102.6 nm contains H Lyman-β (102.57 nm) formed by resonance scattering and may contain a contribution from O pumped by the solar Lyman-β line, as occurs in the dayglow of Earth (*2*). The EUV brightness ratio of Lyman-α to the feature at 102.6 nm on Venus is 170, compared to the ratio of 624 measured by the EUV in the interplanetary hydrogen background. Also visible are lines of He (58.4 nm) and $O^+$ (83.4 nm), confirming earlier reported detections made with EUV instruments on Mariner 10 (*3*) and Venera 11 and 12 (*4*). The He line at 58.4 nm is due to resonance scattering of sunlight by atomic He. Several mechanisms can contribute to the formation of $O^+$ at 83.4 nm: direct photoionization excitation of atomic oxygen, electron impact ionization and excitation of atomic oxygen, and resonance scattering of sunlight by oxygen ions (*5*).

Other Venus emissions were observed in the region from 90 to 120 nm (Fig. 1); they are presumably an unresolved blend of several atomic or molecular emissions or both. The dayglow of Earth contains numerous oxygen and nitrogen emissions in this region (*5*). The strongest unresolved line in the Venus EUV spectrum is probably O (98.9 nm), prominent in the dayglow of Earth, (*6*) where it is excited by photoelectron impact (*5*). Table 1 indicates the derived brightnesses for the resolved and nearly resolved lines and compares the values to ones obtained with EUV instruments on Mariner 10 (*3*) and Venera 11 and 12 (*4*). Galileo brightness values represent the averages over the portion of the sunlit disk viewed by the instrument, whereas Mariner and Venera brightness values represent the largest value seen on the planet. Error estimates for the Galileo data are based on the uncertainties in the absolute calibration of the EUV in the laboratory.

For the Lyman-α measurements made during the interplanetary cruise period, the great circle swept out by the EUV sampled

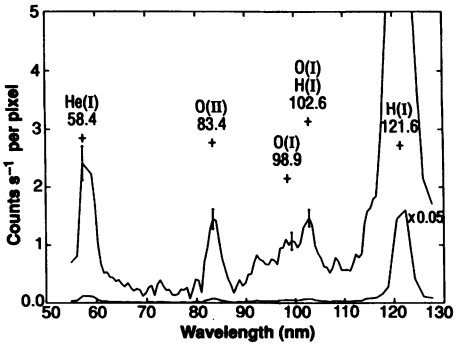


**Fig. 1.** The EUV spectrum of Venus. Error bars (±1 σ) have been placed on identified lines.

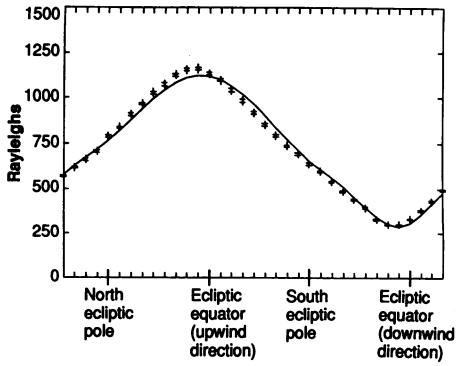


**Fig. 2.** Interplanetary Lyman-α observations for a great circle at an ecliptic longitude of 252° passing through the ecliptic poles. The observations are marked with double pluses, which indicate the ±1 σ limits. The model results are shown by the solid line.

the sky in 35 10° sectors that are 0.87° wide. As the spacecraft orbited the sun its spin axis was kept near the sun, so the EUV observation path systematically changed in ecliptic longitude. The entire celestial sphere was mapped twice during one orbit about the sun. Although Earth-orbiting spacecraft such as OGO-5 (*7*) and planet-orbiting spacecraft such as Pioneer Venus have made extensive maps of the interplanetary Lyman-α emissions, observations from Galileo have the added dimension of a varying heliocentric distance.

The general features of the interplanetary Lyman-α emissions are explained by the interstellar wind model (*8*). In this model, neutral hydrogen atoms of the local interstellar medium enter the solar system because of the relative motion of the sun with respect to the interstellar medium. The neutral hydrogen atoms are ionized by the solar wind and solar ultraviolet radiation, creating a cavity with distinct upwind and downwind directions. The remaining hydrogen atoms scatter solar Lyman-α radiation, producing the interplanetary Lyman-α emissions. The hydrogen cavity is axially symmetric with respect to the incoming velocity vector, provided that the solar ultraviolet flux and solar wind flux are latitudinally invariant. Pioneer Venus observations made at solar minimum in 1986 indicated that the solar wind flux is latitudinally asymmetric, with the rate of ionization being 30% less over the solar poles than that in the ecliptic (*9, 10*).

An important set of interplanetary Lyman-α observations were made with the Galileo EUV in July 1990. The spacecraft was at a heliocentric distance of 1.2 AU and an ecliptic longitude of 342°. The spacecraft attitude was held in a fixed inertial position from day 186 to day 200. During this period, the EUV scanned a complete great circle that intercepted the ecliptic equator at ecliptic longitudes of 252° and 72° near the upwind and downwind directions of the interplanetary atomic hydrogen cavity. The EUV data were continuously integrated onboard the spacecraft and then read out on days 190, 193, 197, and 200. The data from day 190 are shown in Fig. 2. The interplanetary Lyman-α intensity reaches a maximum in the upwind direction just north of the ecliptic equator and a minimum in the downwind direction slightly south of the ecliptic equator.

Two major modifications were made to the interstellar wind model (*10*) to obtain the fit to the data from day 190 shown in Fig. 2. First, the solar wind flux was assumed to be symmetric, with the rate of ionization over the poles being equal to the rate in the ecliptic. A more symmetric flux for the 1990 observations, made at solar maximum, compared with the 1986 Pioneer Venus observations, made at solar minimum, is consistent with the expected dependence of the solar wind on solar activity (*11*). Second, the solar Lyman-α was given a latitudinal dependence with less Lyman-α emanating from the solar poles than that from the solar equator. This latitude effect had been theoretically predicted to occur near solar maximum because of the presence of Lyman-α–emitting active regions at low solar latitudes (*12*). The polar Lyman-α flux 1 AU from the sun, derived with the theory in (*12*), was $2.8 \times 10^{11}$ photons $cm^{-2}\ s^{-1}$, compared to equatorial values that ranged from $3.5 \times 10^{11}$ to $4.1 \times 10^{11}$ photons $cm^{-2}\ s^{-1}$. The range of values for the solar equatorial flux comes from the presence of strong, low-latitude active regions at particular solar longitudes.

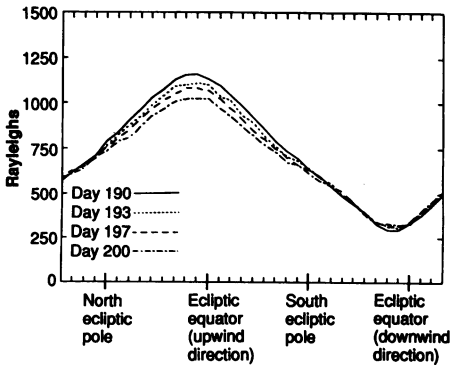


**Fig. 3.** Interplanetary Lyman-α observations for four different time periods, viewed from the same great circle as that in Fig. 2.

Figure 2 has a slight asymmetry between the data and the model, with the data lying above the model in the northern ecliptic hemisphere and below the model in the southern ecliptic hemisphere. This discrepancy is interpreted as a further asymmetry in the solar Lyman-α flux, with the solar flux being more intense in the solar northern hemisphere than that in the solar southern hemisphere at the time of these observations.

The observations from days 190, 193, 197, and 200 are shown in Fig. 3. These observations were all made along the same great circle, which includes the two ecliptic poles and the ecliptic equator in the upwind and downwind directions. The major difference between these four observations of the Lyman-α sky background is the systematic decrease in intensity in the upwind direction in the time period from day 190 to day 200. This change in the Lyman-α sky background is caused by the change in the solar Lyman-α flux during this period. In the upwind direction, the centroid of the volume emission rate of the Lyman-α radiation that is scattered by interplanetary atomic hydrogen is located about 2 AU from the sun. This changing Lyman-α sky background was compared to a solar Lyman-α index derived from Solar Mesosphere Explorer observations of the solar Lyman-α flux made during the previous solar cycle (*13*). This comparison showed that the phase relationship between the observed Lyman-α sky background and the solar Lyman-α index was in agreement with the geometry of the interstellar wind model.

**Table 1.** Features in the dayglow of Venus. Galileo, 8 February 1990; Mariner 10, 5 February 1974; Venera 11, 25 December 1978; and Venera 12, 21 December 1978.

| Wavelength (nm) | Species | Brightness (Rayleighs) | | | |
|---|---|---|---|---|---|
| | | Galileo | Mariner 10 | Venera 11 | Venera 12 |
| 58.4 | He(I) | 200 ± 60 | 600 | 280 | 270 |
| 83.4 | O(II) | 180 ± 60 | | 156 | |
| 98.9 | O(I) | 130 ± 30 | | | |
| 102.6 | H(I), O(I) | 270 ± 60 | | | |
| 121.6 | H(I) | 46000 ± 10000 | 19000 | | |



REFERENCES AND NOTES

1. C. W. Hord *et al.*, *Space Sci. Rev.*, in press.
2. R. R. Meier, D. E. Anderson, Jr., L. J. Paxton, R. P. McCoy, *J. Geophys. Res.* **92**, 8767 (1987).
3. A. L. Broadfoot, S. Kumar, M. J. S. Belton, M. B. McElroy, *Science* **183**, 1315 (1974).
4. J. L. Bertaux *et al.*, *Planet. Space Sci.* **29**, 149 (1981).
5. R. R. Meier, *Space Sci. Rev.*, in press.

6. E. P. Gentieu, P. D. Feldman, R. R. Meier, *Geophys. Res. Lett.* **6**, 325 (1979).
7. G. E. Thomas, *Annu. Rev. Earth Planet. Sci.* **6**, 173 (1978).
8. P. W. Blum and H. J. Fahr, *Astron. Astrophys.* **4**, 280 (1970).
9. R. Lallement and A. I. Stewart, *ibid.* **227**, 600 (1990).
10. J. M. Ajello, *J. Geophys. Res.* **95**, 14855 (1990).
11. A. Hundhausen, private communication.
12. J. W. Cook, R. R. Meier, G. E. Brueckner, M. E. VanHoosier, *Astron. Astrophys.* **97**, 394 (1981).
13. G. J. Rottman and C. A. Barth, *Eos* **71**, 1484 (1990).

26 April 1991; accepted 9 August 1991

# Transcriptional Repression Mediated by the WT1 Wilms Tumor Gene Product

STEPHEN L. MADDEN, DONNA M. COOK, JENNIFER F. MORRIS, ANDREA GASHLER, VIKAS P. SUKHATME, FRANK J. RAUSCHER III*

**The *wt1* gene, a putative tumor suppressor gene located at the Wilms tumor (WT) locus on chromosome 11p13, encodes a zinc finger–containing protein that binds to the same DNA sequence as EGR-1, a mitogen-inducible immediate-early gene product that activates transcription. The transcriptional regulatory potential of WT1 has not been demonstrated. In transient transfection assays, the WT1 protein functioned as a repressor of transcription when bound to the EGR-1 site. The repression function was mapped to the glutamine- and proline-rich $NH_2$-terminus of WT1; fusion of this domain to the zinc finger region of EGR-1 converted EGR-1 into a transcriptional repressor.**

THE SEARCH FOR THE WILMS TUMOR (WT) gene on chromosome 11p13 has yielded a complementary DNA (cDNA) clone (WT1) that has characteristics of a tumor suppressor gene (*1, 2*). The *wt1* gene is mutated or deleted in a subset of sporadic and hereditary Wilms tumors (*2, 3*) and is expressed in the condensing mesenchyme, renal vesicle, and glomerular epithelium of developing kidney, suggesting that WT1 functions in normal kidney differentiation (*4*). The *wt1* gene encodes a protein that contains four zinc fingers and a glutamine- and proline-rich $NH_2$-terminus, structural motifs associated with sequence-specific binding to DNA, and transcriptional regulatory functions (*5*).

The *wt1*-encoded protein recognizes the same DNA sequence element (5′-CGCCCCGC-3′) as the EGR-1 protein, a transcription factor that contains three zinc fingers and shares >65% amino acid sequence similarity with WT1 in the zinc finger region (*6*). After induction by a variety of cell surface stimuli, EGR-1 (also known as NGFI-A, T1S-8, Krox 24, and zif268) (*7, 8*) rapidly accumulates in the nucleus, binds to the EGR site, and activates the transcription of target genes whose products are required for mitogenesis and differentiation (*9, 10*). The proteins encoded by all members of the EGR family are positive activators of transcription when bound to their cognate sequence in target genes (*9, 10*).

To determine the function of WT1 in transcriptional regulation when it is bound to the EGR site, transient transfection assays were carried out with expression vectors (Fig. 1A) that contained the full-length coding region of *wt1* (CMV-WT1) and *egr-1* (CMV–EGR-1) under the control of the cytomegalovirus immediate-early promoter (*11*). As controls, stop codons were introduced into the coding regions of each gene to generate the plasmids CMV-WT1 (TGA) and CMV–EGR-1 (TGA). Of the two reporter plasmids used in these experiments (Fig. 1A), the first contained three synthetic EGR binding sites upstream of the minimal c-*fos* promoter (*10*) linked to the chloramphenicol acetyltransferase (CAT) gene (p3XEBS-CAT), whereas the second contained 1 kb of the murine EGR-1 promoter (*12*) upstream of the CAT gene (pEGR-1.1.2-CAT).

Analysis of CAT activity (*13–15*) in NIH 3T3 fibroblasts cotransfected with the expression and reporter plasmids revealed the expected stimulation of the p3XEBS-CAT vector by CMV–EGR-1 (*10*), but not by the control CMV–EGR-1 (TGA) (Fig. 1B). However, the basal level of transcription was reduced in cells cotransfected with CMV-WT1 and p3XEBS-CAT (Fig. 1B). Neither CMV–EGR-1 nor CMV-WT1 affected a CAT reporter plasmid that lacked EGR binding sites (*16*).

To determine whether WT1 inhibited the ability of EGR-1 to activate p3XEBS-CAT, varying ratios of the CMV-WT1 and CMV–EGR-1 plasmids were cotransfected with p3XEBS-CAT (Fig. 1B). At a 1:1 ratio of CMV-WT1 and CMV–EGR-1, activation by EGR-1 was reduced, and at a 2:1 ratio, activation by EGR-1 was abolished. Thus, WT1 repressed both basal and EGR-1–induced transcription from p3XEBS-CAT. The same experiments performed in human embryonic kidney–derived 293 cells revealed transcriptional activation of the p3XEBS-CAT reporter plasmid by CMV–EGR-1 and repression by CMV-WT1 (Fig. 1B).

The p3XEBS-CAT reporter plasmid contains EGR binding sites in an artificial promoter context and exhibits a low basal level of transcriptional activity (Fig. 1B). This low basal level made it difficult to assess the potency of WT1 as a transcriptional repressor in cotransfection assays (Fig. 1B). To circumvent this problem, we used the pEGR-1.1.2 promoter, which contains several EGR binding sites of varying affinities as well as other genetic regulatory elements (*12*) in their natural context. The WT1 vector efficiently repressed the normal, high basal levels of transcriptional activity of pEGR-1.1.2-CAT in NIH 3T3 cells (Fig. 1C), independent of whether the cells were incubated in high (10%) or low (0.5%) serum after transfection (*16*).

The WT1 mRNA transcript is subject to alternative splicing (*1, 2, 17*) (Fig. 2A), in one case resulting in the insertion of lysine, threonine, and serine (KTS) between the third and fourth zinc fingers. A WT1 protein that contains this insertion does not bind to the EGR-1 site (Fig. 2B) (*6*). A second alternative splice results in the insertion of 17 amino acids in the region immediately $NH_2$-terminal to the zinc finger domain (*1, 17*) and does not affect DNA binding activity (Fig. 2B). To determine the effect of these amino acid insertions on the ability of WT1 to repress transcription, the four possible combinations of the spliced variants were produced by site-directed mutagenesis (*18*), tested for DNA binding activity (Fig. 2B) (*19*) and expression in COS-1 cells (Fig. 2, legend), and assayed for repression by cotransfection with pEGR-1.1.2-CAT (Fig. 2C). The proteins that contained the KTS insertion (WT1-KTS, WT1-17AA-KTS) did not repress transcription of the reporter plasmid (Fig. 2C) or bind to the EGR-1 site (Fig. 2B). However, repression was observed in the absence (WT1) or the presence (WT1-17AA) of the 17–amino acid insertion. Thus, binding to the EGR-1 site is re-

S. L. Madden, D. M. Cook, J. F. Morris, F. J. Rauscher III, The Wistar Institute of Anatomy and Biology, 3601 Spruce Street, Philadelphia, PA 19104.
A. Gashler and V. P. Sukhatme, Department of Medicine, Molecular Genetics and Cell Biology, Howard Hughes Medical Institute, Chicago, IL 60637.

*To whom correspondence should be addressed.